applied mechanics

Article

A 3D-Printed Honeycomb Cell Geometry Design with Enhanced Energy Absorption under Axial and Lateral Quasi-Static Compression Loads

Marco Menegozzo *, Andrés Cecchini, Frederick A. Just-Agosto, David Serrano Acevedo, Orlando J. Flores Velez, Isaac Acevedo-Figueroa and Jancary De Jesús Ruiz

Department of Mechanical Engineering, University of Puerto Rico at Mayagüez, Mayaguez, PR 00681, USA; andres.cecchini@upr.edu (A.C.); frederick.just@upr.edu (F.A.J.-A.); david.serrano@upr.edu (D.S.A.); orlando.flores2@upr.edu (O.J.F.V.); isaac.acevedo@upr.edu (I.A.-F.); jancary.dejesus@upr.edu (J.D.J.R.)
* Correspondence: marco.menegozzo@upr.edu; Tel.: +1-787-832-4040

Abstract: This work presents an innovative honeycomb cell geometry design with enhanced in-plane energy absorption under quasi-static lateral loads. Numerical and experimental compression tests results under axial and lateral loads are analyzed. The proposed cell geometry was designed to overcome the limitations posed by standard hexagonal honeycombs, which show relatively low stiffness and energy absorption under loads that have a significant lateral component. To achieve this, the new cell geometry was designed with internal diagonal walls to support the external walls, increasing its stiffness and impact energy absorption in comparison with the hexagonal cell. 3D-printed unit-cell specimens made from ABS thermoplastic material were subjected to experimental quasi-static compression tests, in both lateral and axial directions. Energy absorption was compared to that of the standard hexagonal cell, with the same mass and height. Finite element models were developed and validated using experimental data. Results show that the innovative geometry absorbs approximately 15% more energy under lateral compression, while maintaining the same level of energy absorption of the standard hexagonal cell in the axial direction. The present study demonstrates that the proposed cell geometry has the potential to substitute the standard hexagonal honeycomb in applications where significant lateral loads are present.

Keywords: honeycomb; cell geometry; sandwich panels; energy absorption; lateral loads; 3D-printing

Citation: Menegozzo, M.; Cecchini, A.; Just-Agosto, F.A.; Serrano Acevedo, D.; Flores Velez, O.J.; Acevedo-Figueroa, I.; De Jesús Ruiz, J. A 3D-Printed Honeycomb Cell Geometry Design with Enhanced Energy Absorption under Axial and Lateral Quasi-Static Compression Loads. *Appl. Mech.* **2022**, *3*, 296–312. https://doi.org/10.3390/applmech3010019

Received: 16 February 2022
Accepted: 12 March 2022
Published: 14 March 2022

1. Introduction

In the last decades, the structural design approach used in the aerospace, naval and automotive areas has been aiming to obtain minimum weight, and on the other hand, maximum structural safety. To meet these two conflicting objectives, sandwich panel honeycomb cores are widely used. The advantages offered by such structures consist of a light weight, high strength-to-weight ratio, high stiffness-to-weight ratio and high energy absorption capabilities [1]. Honeycomb geometries are typically built up of cells of constant cross section, such as in the case of the standard hexagonal honeycomb. When loaded along the direction of the cells' axes, the hexagonal honeycomb offers high values of energy absorption and stiffness. The mechanical energy of axial loads is absorbed by plastic deformation of the honeycomb during the compression crushing. However, the standard prismatic honeycomb geometry possesses limited stiffness and energy absorption when undergoing loads that present a substantial lateral component, such as lateral compression. Such kinds of loads represent possible scenarios that should be taken into consideration when designing sandwich cores for structures that can experience non-axial loads due to potential impacts with foreign objects or fatigue, such as ship hulls, aircraft fuselages and engine cases, as well as terrestrial vehicles.

As an alternative to prismatic honeycombs, numerous lattice geometries have been proposed and studied in the last years. These include architected and origami-inspired structures, pre-folded thin-walled tubes, cross-chiral and hierarchical cellular structures, to name a few. Current 3D-printing technologies allow these geometries to be manufactured at a relatively high speed and low cost using different materials (e.g., thermoplastics, thermoset resins, fiber reinforced plastics, etc.). 3D-printed specimens have been fabricated and tested under a variety of loading conditions, including in-plane and out-of-plane quasi-static and dynamic compression, shear, three-point bending and impact, with the objective to characterize their mechanical behavior and structural performance. To this end, numerous studies have been conducted in the last few years. Chen et al. [2] investigated the in-plane compressive stiffness, energy absorption and failure modes of 3D-printed hierarchical cellular structure. McCaw and Cuan-Urquizo [3] experimentally studied the mechanical properties of non-planar auxetic and disrupted sinusoidal lattice structures under quasi-static cyclic loading. Li et al. [4] studied the compressive behavior of 3D-printed auxetic reinforced composites, while Townsend et al. [5] presented a new 3D-printed thermoplastic polyurethane fold origami honeycomb design with tailored out-of-plane energy absorption behavior. Bates et al. [6] explored the effect of grading methodologies on the energy absorption and damping behavior of 3D-printed flexible thermoplastic polyurethane honeycombs under quasi-static, cyclic and impact loadings. Andrew et al. [7] experimentally investigated the in-plane and out-of-plane compression energy absorption and piezoresistive-self-sensing performance of 3D-printed discontinuous carbon fiber-reinforced polyetheretherketone cellular composites. Ma et al. [8] studied the performance of a kirigami-inspired pyramid foldcore sandwich structure subjected to quasi-static out-of-plane compression and shear loads. Wang et al. [9] investigated the mechanical response of 3D cross-chiral structures under uniaxial compression using experiments, FE models and theoretical analysis. Yang et al. [10] analyzed the energy absorption of 3D-printed thin-walled tubes with pre-folded origami patterns under uniaxial loading. Li et al. [11] determined the in-plane compression strength and energy absorption of polylactic acid (PLA) 3D-printed wood-inspired hierarchical honeycombs under quasi-static and dynamic loads. The effect of geometric parameters and material properties on the structural performance of 3D-printed honeycombs and sandwich panels have also been investigated. Qi et al. [12] studied the influence of structural parameters on the low-impact response and energy absorption characteristics of ABS-like resin 3D-printed origami-inspired honeycombs. Guo et al. [13] investigated the influence of geometric morphology on mechanical properties, peak force, energy absorption and damage mode of 3D-printed negative Poisson's ratio convex-concave honeycomb tubes under quasi-static and dynamic compression. Zaharia et al. [14] conducted elasto-plastic FE analysis on 3D-printed lightweight thermoplastic sandwich structures with diamond cell honeycombs and corrugated cores to evaluate their failure modes under compression, three-point bending and tensile test. Basurto et al. [15] also studied the effect of process parameters on mechanical properties and energy absorption of 3D-printed polyethylene terephthalate glycol honeycombs under in-plane compression tests. In a similar study, Mansour et al. [16] investigated the mechanical performance of 3D-printed second-order hierarchical ABS honeycomb structures with carbon fiber and carbon nanotube reinforcements under compression and cyclic compression testing.

Particularly, energy absorption and failure mechanisms of 3D-printed lightweight honeycombs under low-velocity impact loading are receiving increasing attention due to their enormous potential for aerospace structural applications. Sarvestani et al. [17,18] determined the significant effect of core topology and geometrical parameters on failure mechanism and energy absorption of 3D-printed meta-sandwich structures subjected to quasi-static three-point bending and low-velocity impact tests. They also studied the energy absorption capability of 3D-printed PLA lightweight sandwich panels with architected cellular cores under low-velocity impact. Özen et al. [19] also investigated the low-energy impact response of woven CFRP sandwich composite panels with 3D-printed thermoplastic

ABS honeycomb and re-entrant cores, particularly their impact strength and energy dissipation behavior. Chen et al. [20] performed a similar analysis on additive manufactured 3D re-entrant honeycombs under impact and quasi-static compression loading, in order to determine their energy absorption capability and failure modes. Ma et al. [21] also conducted static and impact compression analyses to study the deformation behavior and energy absorption of composite re-entrant honeycomb cylindrical shells.

From the aforementioned studies, the following findings were observed: (1) Process and geometric parameters can be modified to tailor the mechanical properties and structural response of 3D-printed honeycombs, and core topology has a significant effect on energy absorption and failure mechanisms of the structure; (2) Hierarchical and auxetic lattice structures show superior energy absorption than conventional honeycombs, but also show a reduction in stiffness; and (3) Even though many honeycomb and lattice geometries have been proposed, there is not a general consensus on which is the best alternative for crashworthiness applications.

In order to increase the impact energy absorption of 3D-printed honeycombs under lateral loads, a new cell structure was designed with an external square shape containing internal diagonal walls that are neither parallel nor perpendicular to the cells' axes. The particular orientation of the diagonal walls allows an increase of the stiffness and energy absorption along the lateral directions, and allows the load to be transferred through alternative paths, independently from the direction of the external forces acting on the cell. The energy absorption capability of a unit cell tailored with the innovative geometry was then compared to the standard hexagonal honeycomb cell with the same mass and height. Both the innovative and standard cells were subjected to quasi-static compression tests, both axially and laterally. Finite element (FE) models were developed and validated using experimental results. The axial compression results proved that the new cell geometry maintains the same level of energy absorption of the standard hexagonal cell, while the lateral compression tests indicated that the innovative cell geometry can absorb approximately 15% more energy than the standard hexagonal one.

2. Materials and Methods

2.1. Cell Geometry Design

The innovative cell geometry design proposed in this paper is based on the following two requirements: (1) The need to increase the energy absorption of conventional honeycomb structures under lateral compression; and (2) The ability to assemble multiple cells into a compact rectangular arrangement without the necessity of cutting the panel edges, as it occurs in the case of standard hexagonal honeycombs. To satisfy the aforementioned requirements, the innovative cell was designed with a square cuboid external shape containing internal diagonal walls, i.e., walls that lie in planes that are neither parallel nor perpendicular to the cell axis, as depicted in Figure 1a,b. With this geometric configuration, the cell vertical walls will transfer the vertical load, while the internal diagonal walls will transfer the load in the in-plane direction, thus improving the energy absorption capability observed in prismatic cells. Initially, a honeycomb geometry constituted of tetrahedral cells was considered, but it was subsequently discarded, as it was not possible to assemble them into the desired shape without leaving any void spaces. Therefore, the cell geometry proposed in this work, which is composed of four hexahedral sub-cells that for a parallelepiped-shaped cell, was adopted, as it represents the simplest design solution that satisfies the two design requirements. Innovative cells with the same size can be stacked together in two different geometric configurations (where the different patterns only differ for the mutual orientation of the cells), as shown in Figure 1c, to form square or rectangular honeycomb panels. Figure 2 depicts the innovative cell cross section at 25, 50 and 75 percent of the cell height.

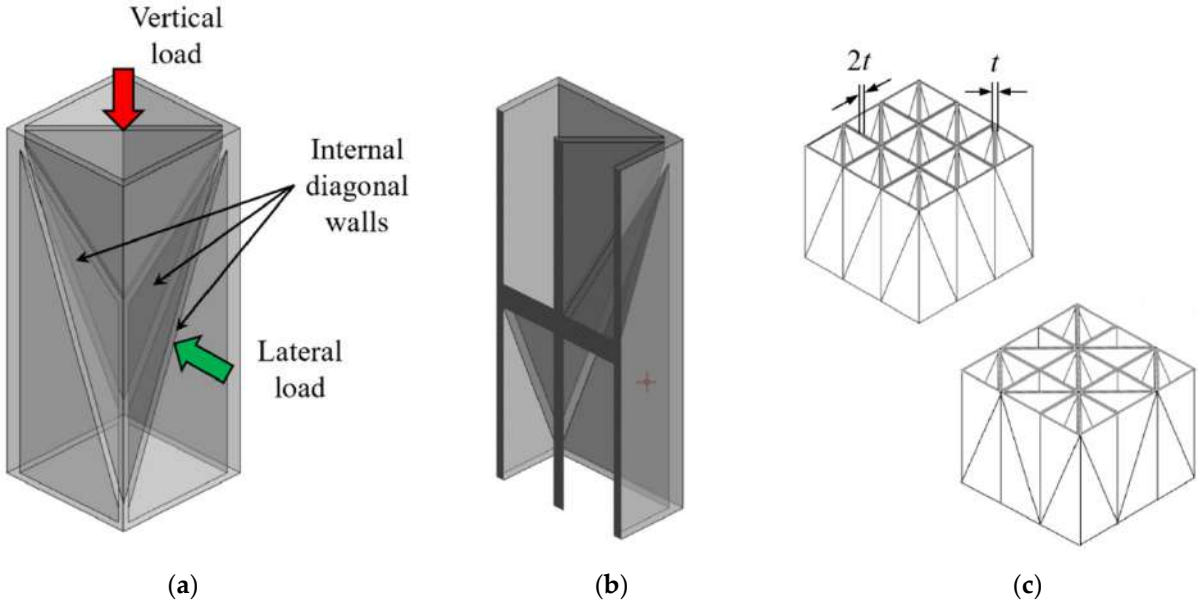

Figure 1. (**a**) Innovative cell geometry with internal diagonal walls; (**b**) cell cross-sectional view; and (**c**) two possible geometric honeycomb configurations, where the thickness of the external vertical walls is twice the thickness of the internal diagonal walls (t).

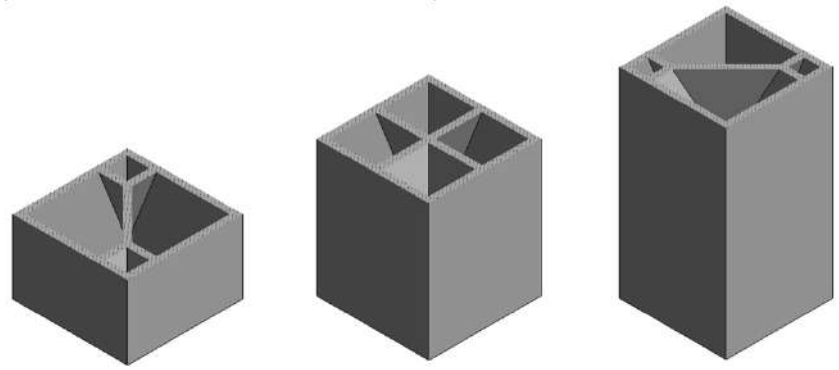

Figure 2. Innovative cell cross section at 25, 50 and 75 percent of the cell height.

To compare the energy absorption under both an axial and lateral compressive load, the innovative cell and the hexagonal standard cell were dimensioned in such a way that they had the same height and mass. In order to design the innovative and standard hexagonal cells so that they had the same mass, the innovative cell was dimensioned first, and then the dimensions of the standard hexagonal cell were determined accordingly. The following dimensions were selected for the innovative cell geometry: thickness of 1.5 mm, side length of 25.4 mm and height of 63.5 mm. Once the corresponding material volume was calculated (13,262 mm^3), the same material volume and mass were assigned to the standard honeycomb cell. To determine the remaining dimensions of the standard hexagonal cell, the wall length was assigned a value of 13.7 mm, and the wall thickness was obtained using the following relation [22]

$$\frac{V_s}{V_t} = \frac{2}{\sqrt{3}}\left(\frac{2t}{l}\right) \tag{1}$$

where V_s and V_t represent the volume of the innovative cell (13,262 mm^3) and the volume of the solid (completely filled with material) hexagonal cell ($V_t = 3\sqrt{3}l^2h/2$), respectively. In Equation (1), t is the cell wall thickness and l is the cell wall length. The resulting standard hexagonal cell wall thickness was 2.5 mm. The volume fractions of the standard

and innovative cells were 0.42 and 0.30, respectively. The dimensions of both cells are shown in Figure 3.

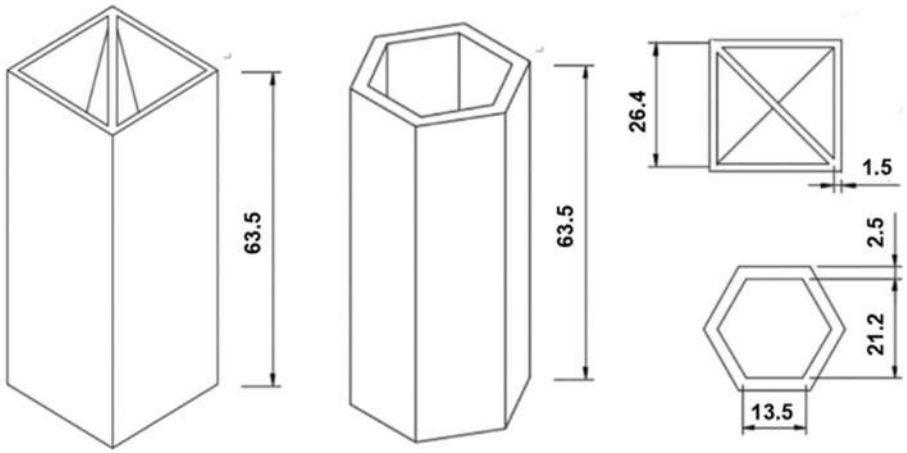

Figure 3. Dimensions (in mm) of innovative and standard hexagonal cells specimens for testing.

2.2. Materials and Fabrication

The test specimens were manufactured from white ABS (Acrylonitrile-Butadiene-Styrene) thermoplastic polymer using a Zortrax M300 fused filament deposition 3D printer (Zortrax Company, Olsztyn, Poland). The isotropic bulk material properties of ABS, determined from the manufacturer datasheet, were a density of 1040 kg/m^3, elastic modulus of 2 GPa, yield strength of 25 MPa and Poisson's ratio of 0.3. The printing orientation was chosen in such a way that the cross-sectional area of the cell was seated on the printing bed. All specimens were printed with the same orientation to maintain consistency. The printing parameters used in the manufacturing process were the following: filament diameter 1.75 mm, infill density 60%, layer thickness 0.14 mm, printing speed 80 mm/s, extruder temperature 230–250 °C and bed temperature 70–110 °C. The resulting printed specimens are shown in Figure 4, in which the infill printing pattern can be observed.

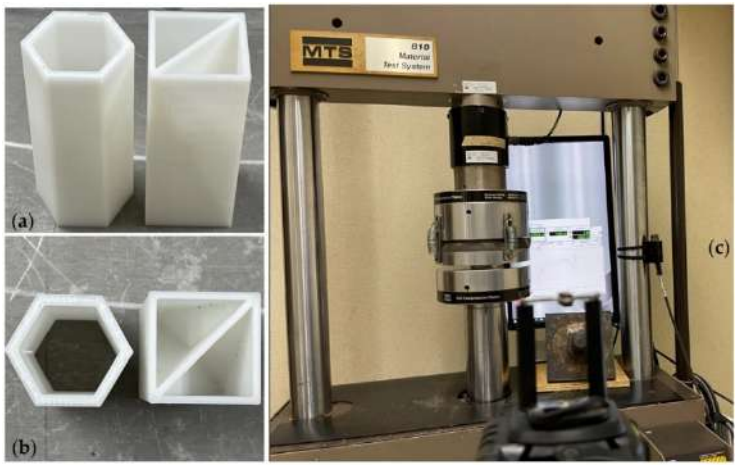

Figure 4. (**a**) 3D-printed test specimens. (**b**) 3D-printed specimens infill printing pattern. (**c**) Quasi-static compression testing system.

2.3. Experimental Setup

Quasi-static compression tests were performed on 3D-printed ABS specimens using an MTS 810 Servo-Hydraulic Material Test System with a maximum load capacity of 200 kN and maximum displacement of 76.2 mm (see Figure 4). The 3D-printed cells were placed between the two circular platens and compressed at a displacement rate of 0.85 mm/min.

For the axial compression tests, the total compressive displacement was 45.7 mm, which represents the 72% of the cell height. For the novel and hexagonal cells under lateral compression, the total compressive displacement was 22.8 mm, which represents 82% and 87% of the novel cell wall length and hexagonal cell minimal diameter, respectively. The loading process was recorded by a standard digital camera and the experimental force versus displacement data was extracted from the testing machine. To obtain reliable results, three specimens of each cell geometry and loading direction were tested.

2.4. Numerical Modeling

3D-explicit nonlinear finite element (FE) analysis of the novel honeycomb cell and conventional hexagonal cell under quasi-static compression load was conducted using the commercial software ANSYS Workbench with AUTODYN solver with the objective to replicate the actual tests. The FE models consist of a single-cell honeycomb loaded in either axial or lateral direction, as shown in Figures 5 and 6. The honeycombs were modeled using two solid elements across the thickness and multilinear isotropic hardening material with an elastic modulus of 1.2 GPa, yield strength of 20.5 MPa and density equal to 1040 kg/m^3. The specimens were placed between two rigid plates and subject to a controlled vertical deformation rate. The crushing of the honeycomb cell was accomplished by fixing the lower plate in all directions, while the upper plate moved downward with linear velocity varying from an initial value of zero to a final maximum value. In all cases, the crushing distance was set to be approximately 80% of the original cell length. To balance computational time and solution accuracy, the kinetic energy of the upper plate was maintained below 10% of the internal energy during the simulations, so that dynamic effects can be neglected. The interaction between the specimens and the rigid plates was modeled using frictional contacts with equal static and dynamic coefficients of 0.05. Body self-contact based on the penalty formulation was defined for the honeycomb cell elements. Hourglass energy was controlled using the Flanagan-Belytschko algorithm, with a stiffness coefficient of 0.08 and a viscous coefficient of 0.1. In the case of the model corresponding to the novel cell under lateral load, the mesh was divided in two parts at its mid-plane section. Then, the two parts were connected together using a bonded contact with a shear stress limit of 3.4 MPa. This contact allows the interaction between the parts until it breaks at the specified shear stress limit. The purpose of this contact was to replicate the failure of the cell at the mid-section observed during the actual compression test. The FE model settings are listed in Table 1. From this analysis, reaction force vs. displacement curves and absorbed energy were obtained and compared with the corresponding experimental results.

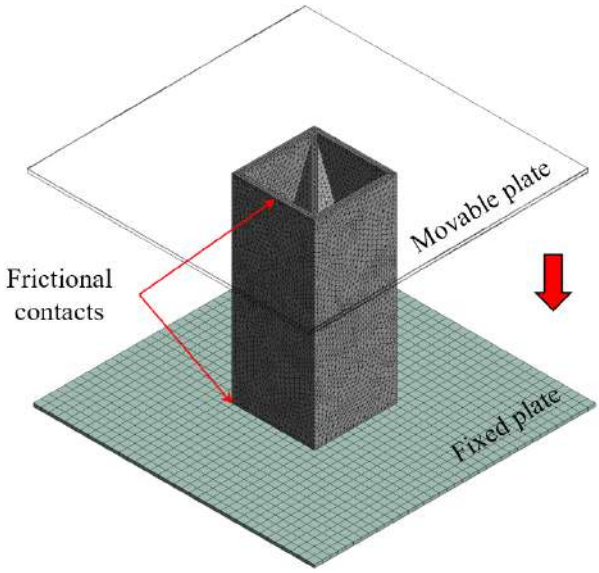

Figure 5. FE model of novel cell under axial load.

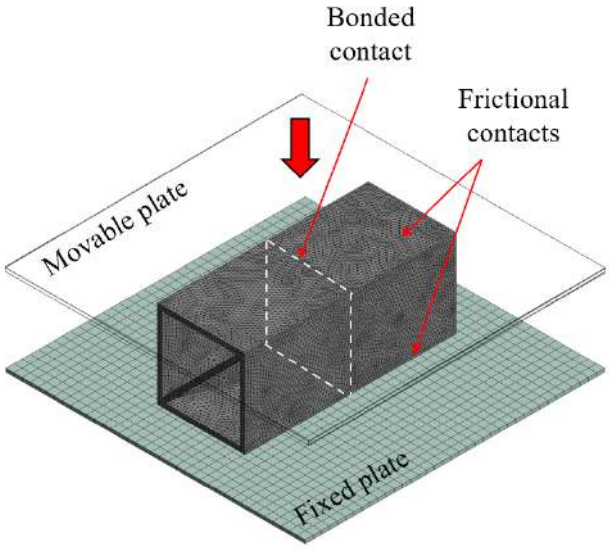

Figure 6. FE model of novel cell under lateral load.

Table 1. FE analysis settings.

Parameter	Setting	Parameter	Setting
Analysis type	Explicit-dynamic/quasi-static	Contact type	Frictional
Material model	Multilinear isotropic hardening	Static friction coeff.	0.05
Elastic modulus	1.2 GPa	Dynamic friction coeff.	0.05
Yield strength	20.5 MPa	Hourglass control	Flanagan-Belytschko
Poisson's ratio	0.3	Stiffness coeff.	0.08
Density	1040 kg/m^3	Viscous coeff.	0.1

3. Results

Quasi-static compression tests were performed on the novel cell geometry and the conventional hexagonal cell under both axial and lateral loads. Three test specimens of each case scenario were manufactured and tested. FE analysis was conducted and validated using experimental results. Experimental load versus displacement curves were plotted for each cell geometry and loading condition. For the case corresponding to axial loading, energy absorption (EA) was computed using Equation (2) for a crushing distance corresponding to 2/3 the initial length (42.3 mm). In a similar fashion, the case corresponding to transverse loading was examined for a crushing distance corresponding to 2/3 the initial width (17.5 mm). The maximum reaction force during the crushing length was also determined in each case. Figure 7 shows the reaction force versus displacement of the novel cell geometry under axial loading. The initial linear elastic response of the novel cell is followed by the sudden crushing of the top end of the specimen, as shown in Figure 8a. Then, the load increases again until the crushing of the bottom end of the specimen occurs. After the second collapse, the reaction force experiences a slight increment, followed by a small reduction. Densification approximately starts after 45 mm of displacement. Figure 9 shows the FE analysis of the novel cell geometry under axial load. In Figure 10, FE results are compared with experimental data showing very good agreement. The averaged experimental absorbed energy and maximum reaction force of the novel cell under axial load were 164.7 J and 6.0 kN, respectively. The specific energy

absorption corresponding to a crushing length of 42.3 mm was 1.17 J/g, which is consistent with the value observed in the hexagonal cell geometry loaded in the axial direction.

$$EA = \int_0^{l_c} F(l)dl \tag{2}$$

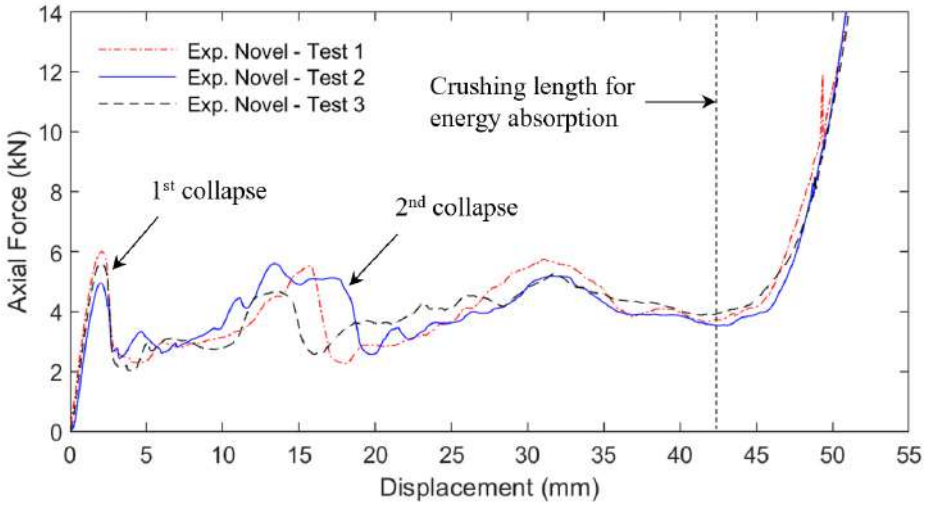

Figure 7. Experimental load vs. displacement curves for novel cell under axial load.

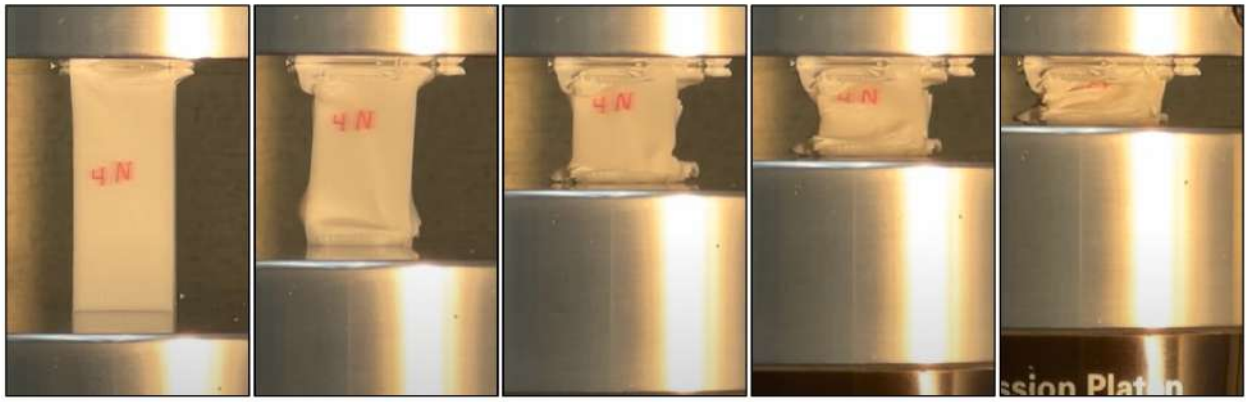

(**a**) (**b**) (**c**) (**d**) (**e**)

Figure 8. Experimental compression test of the novel cell under axial load during the different stages graphed in Figure 7: (**a**) First collapse; (**b**) Second collapse (**c**,**d**) Between 20 mm and 42 mm; and (**e**) Densification.

Figure 9. FE analysis of deformation process for the novel cell under axial load.

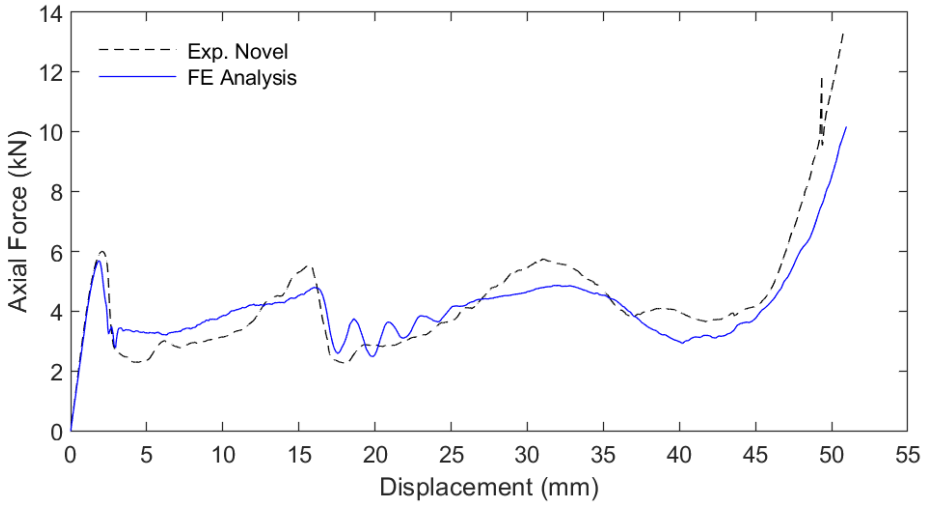

Figure 10. Load vs. displacement curves for novel cell under axial load: comparison between experimental and FEA.

The experimental reaction force versus displacement curves of the novel cell geometry under lateral loading are shown in Figure 11. The initial linear elastic response is followed by the plastic buckling of the vertical cell walls, as shown in Figure 12. Immediately after wall buckling, the cell mid-section fails by shear, which makes the reaction force continue to drop. This failure occurs as a result of the antisymmetric-buckling curvature of the vertical walls, combined with the stress concentration region within the cell observed in the FE model (see Figures 13 and 14). In this case, densification starts after approximately 17 mm of displacement. The maximum shear stress at the mid-section of the novel cell obtained by FE analysis was 17.6 MPa. Figure 15 shows good agreement between FE results and experiments. The averaged experimental absorbed energy and maximum reaction force of the novel cell under lateral load were 27.0 J and 4.8 kN, respectively. The specific energy absorption corresponding to a crushing length of 14.8 mm was 0.19 J/g. The performance of the new cell design under quasi-static compression loading was compared to that of the conventional hexagonal cell. Experimental and FE results are summarized in Table 2. Figure 16 shows the experimental load versus displacement curves of the hexagonal cell under the axial compression test. In this case, the averaged absorbed energy and maximum reaction force were 164.7 J and 6.5 kN, respectively. The specific energy absorption corresponding to a crushing length of 42.3 mm was 1.17 J/g; this demonstrates that the novel cell design and the hexagonal cell have similar performance in the axial direction. Experimental deformation behavior was replicated with very good agreement by the FE model, as shown in Figures 17 and 18. In Figure 19, experimental load versus displacement curve is compared with FE results, showing excellent agreement. In the lateral direction, the hexagonal cell showed an averaged energy absorption of 23.5 J and a maximum reaction force of 2.0 kN. The specific energy absorption, corresponding to a crushing length of 17.5 mm, was 0.16 J/g. Compression test results of the hexagonal cell along the lateral direction are shown in Figure 20. Test specimen 2 experienced wall fracture which can be observed by the sudden drop in the blue curve around the 12 mm compression length. The other two specimens did not show evidence of fracture. Experimental and numerical deformation behaviors are shown in Figures 21 and 22, respectively. The load versus displacement curve obtained from experimental compression test is compared with FEA in Figure 23. The amounts of absorbed energy for the novel and hexagonal cells in both axial and lateral directions are compared in Figure 24. Figure 25 shows a comparison of the initial part of the experimental load versus displacement curves between the novel and the hexagonal cell for both axial and lateral loading conditions.

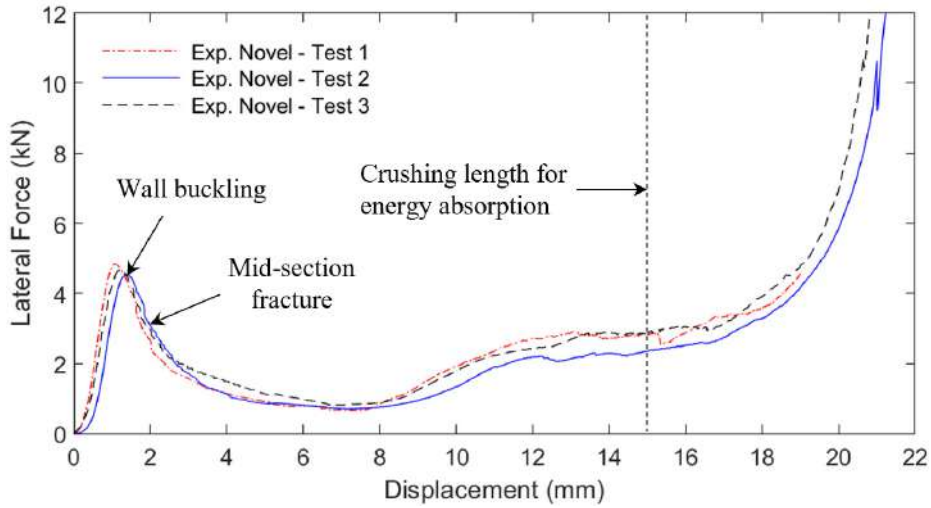

Figure 11. Experimental load vs. displacement curves for novel cell under lateral load.

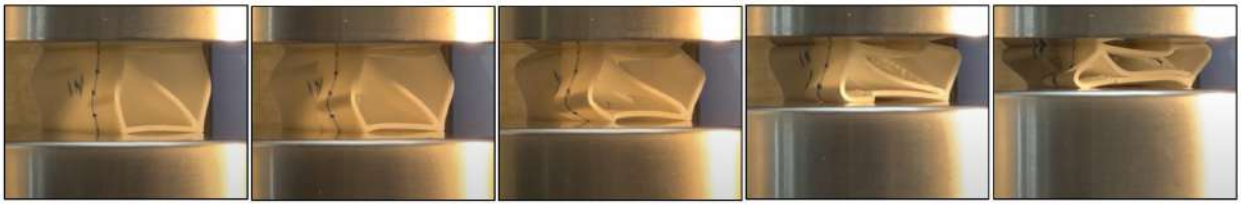

(**a**) (**b**) (**c**) (**d**) (**e**)

Figure 12. Experimental compression test of novel cell under lateral load. (**a**) Wall buckling; (**b**) Mid-section fracture; (**c**) Lower plateau (**d**) Upper plateau; and (**e**) Beginning of densification.

Figure 13. FE analysis of deformation process for the novel cell under lateral load.

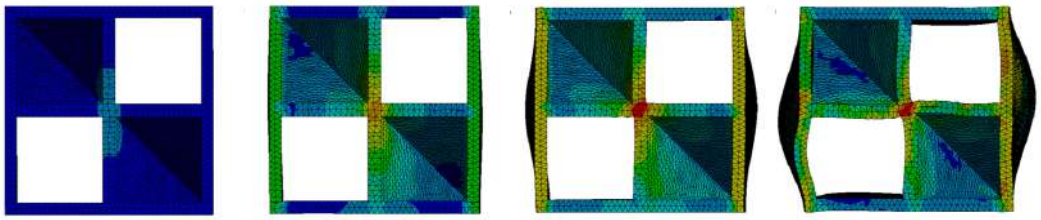

Figure 14. Shear stress concentration at the mid-section of the novel cell.

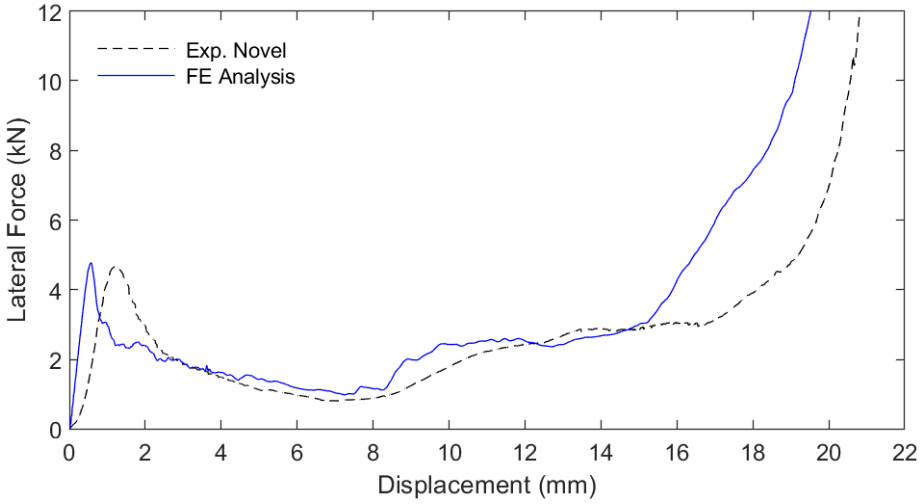

Figure 15. Load vs. displacement curves for novel cell under lateral load: comparison between experimental and FEA.

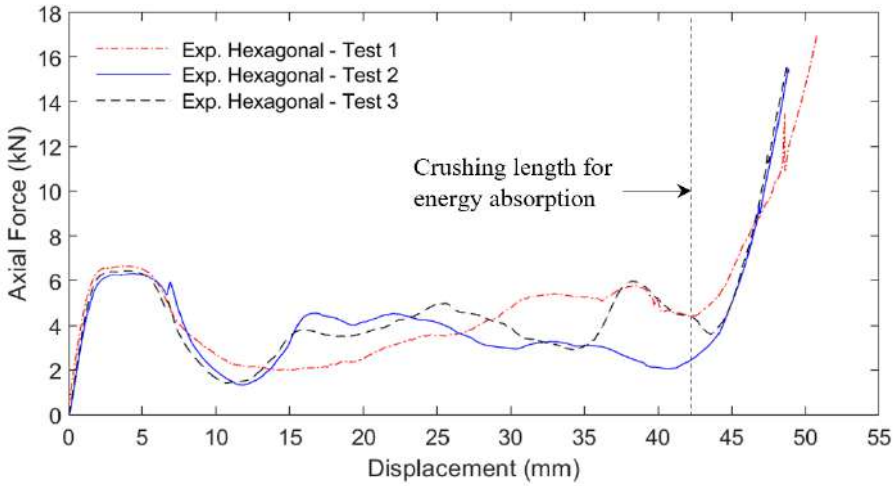

Figure 16. Experimental load vs. displacement curves for hexagonal cell under axial load.

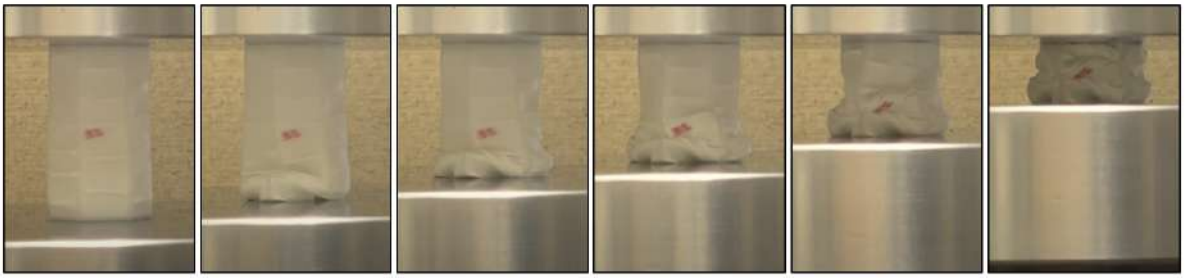

Figure 17. Experimental compression test of standard hexagonal cell under axial load.

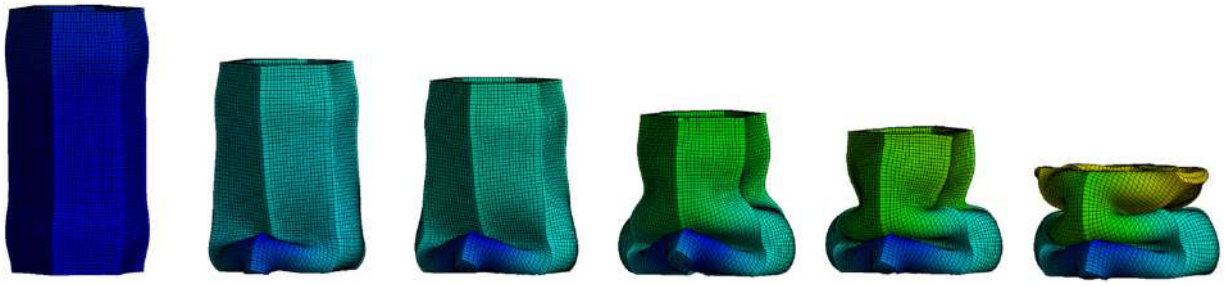

Figure 18. FE analysis of deformation process for the standard hexagonal cell under axial load.

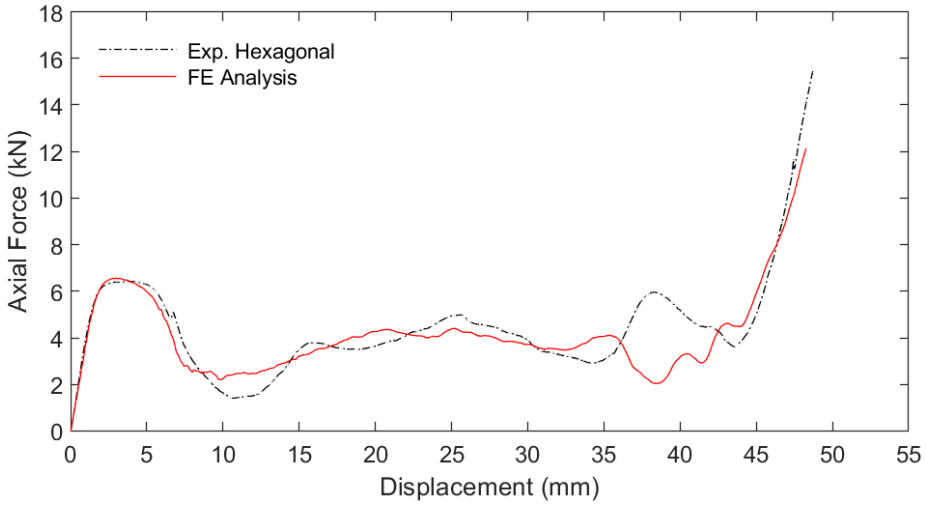

Figure 19. Load vs. displacement curves for hexagonal cell under axial load: comparison between experimental and FEA.

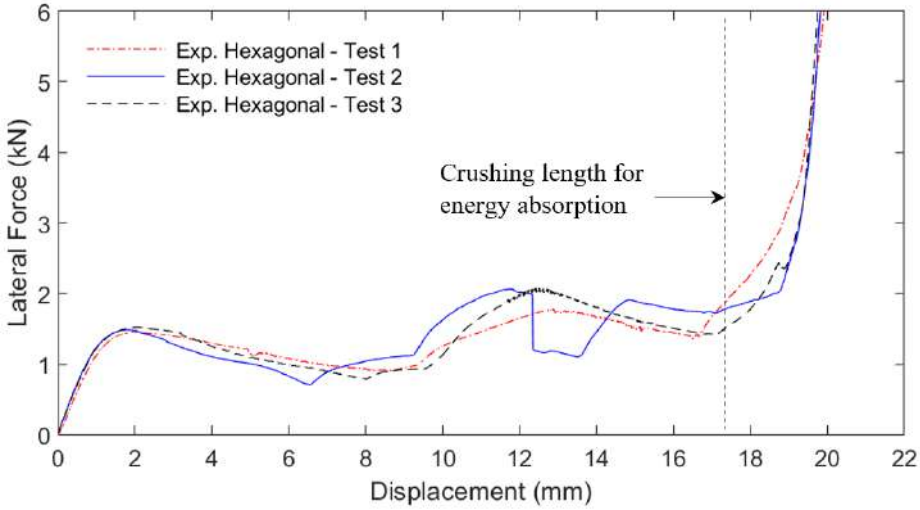

Figure 20. Experimental load vs. displacement curves for hexagonal cell under lateral load.

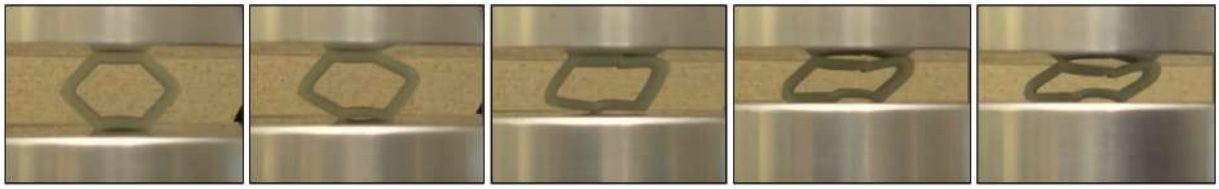

Figure 21. Experimental compression test of standard hexagonal cell under lateral load.

Figure 22. FE analysis of deformation process for the standard hexagonal cell under lateral load.

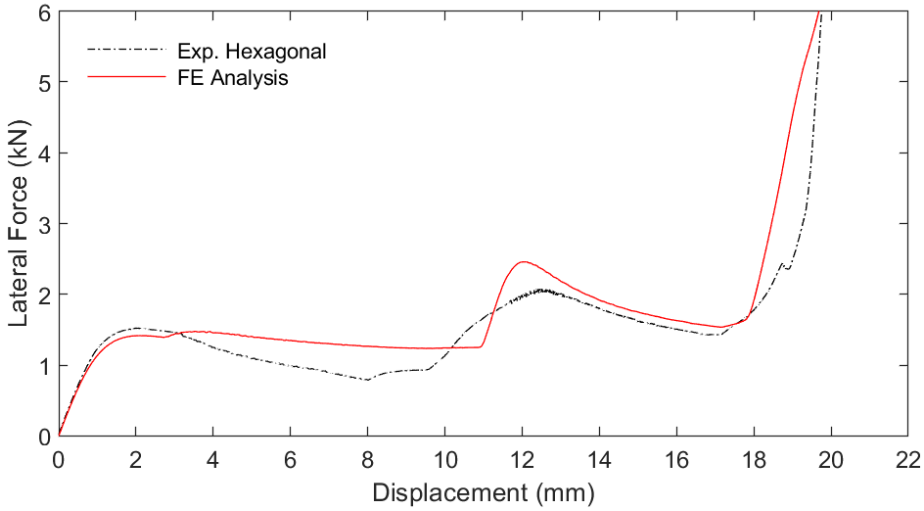

Figure 23. Load vs. displacement curves for hexagonal cell under lateral load: comparison between experimental and FEA.

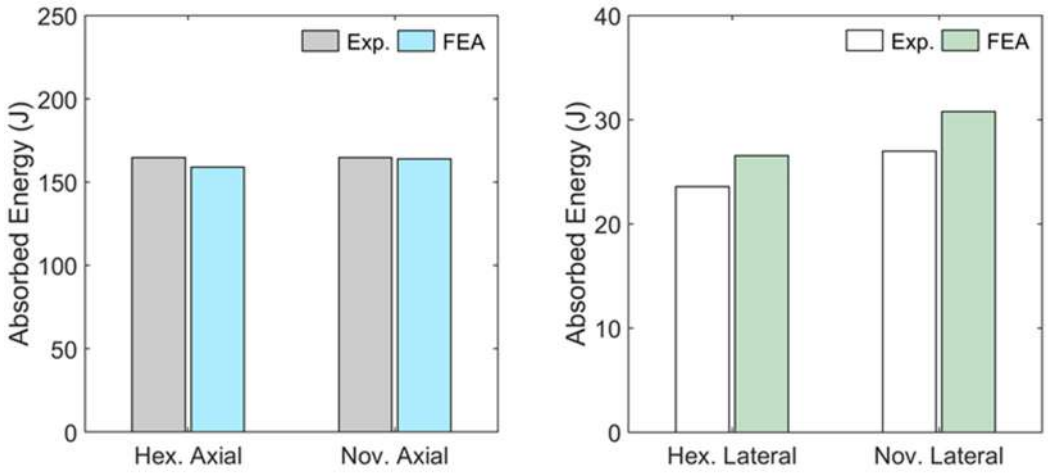

Figure 24. Comparison of the amounts of energy absorbed for novel and hexagonal cells, along the axial direction and along the lateral direction.

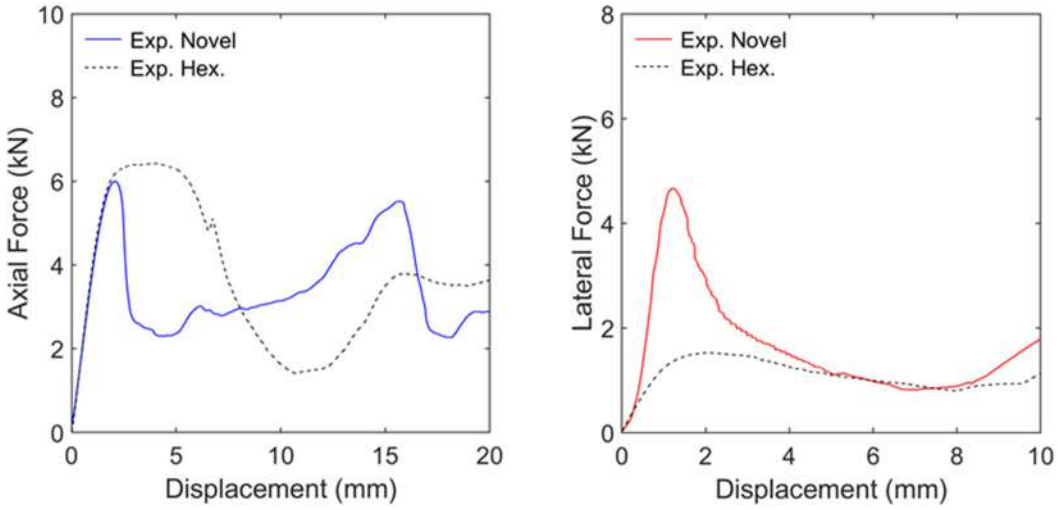

Figure 25. Comparison of load versus displacement curves between novel and hexagonal cells, in the case of both axial force and lateral force.

Table 2. Summary of experimental (average) and FE results. FE results are shown in parentheses (). Energy absorption and maximum force are calculated up to a strain of 2/3.

Cell Geometry (Load Case)	Novel (Axial Load)	Hexagonal (Axial Load)	Novel (Lateral Load)	Hexagonal (Lateral Load)
Energy absorption (J)	164.7 (159.0)	164.7 (163.9)	27.0 (30.7)	23.5 (26.5)
Maximum force (kN)	6.0 (5.6)	6.5 (6.5)	4.8 (4.7)	2.0 (2.4)
Specific energy absorption (J/g)	1.17	1.17	0.19	0.16
Densification length (mm)	45.0	42.5	18.0	18.0
Crushing length for energy absorption (mm)	42.3	42.3	14.8	17.5

4. Discussion

The present study shows that the energy absorption capability of the proposed cell design under quasi-static compression axial load was very similar to that of the conventional hexagonal cell. In the lateral direction, however, the novel cell showed a 15-percent increment in absorbed energy compared to the hexagonal cell. The deformation mechanism observed in the case of the innovative cell under axial load can be divided into three stages: (1) linear elastic buckling of the vertical walls up to the crushing of one end of the cell; (2) plastic compression up to the crushing of the other end of cell; and (3) crushing of the central portion until final densification. Under lateral loading, the deformation pattern observed in the innovative cell is characterized by the following stages: (1) elastoplastic buckling of the cell walls; (2) shear fracture of the cell mid-section due to the antisymmetric cell geometry with respect to the plane at half-height of the cell; and (3) crushing and densification.

Furthermore, the initial capacity of resisting load, which occurs at around 1.8 mm for both cases, increased from 1.6 kN to 4.8kN, as indicated in Figure 25. This value corresponds to 3 times the capacity of the standard hexagonal geometry. In particular, during the first stage of the deformation under lateral load, between 0 mm and 4 mm, the energy absorbed by the novel cell is 100% higher than the energy absorbed by the standard hexagonal cell. In addition, it was found that the novel cell experienced a 4% increment in crushing length before densification in the axial direction when compared to the hexagonal cell. Both cell geometries presented identical crushing lengths before densification in the lateral direction. The failure mechanisms and energy absorption capabilities observed in the unit-cell specimens were the result of both the cell topology and the end effect, which, combined, facilitated the early collapse of the cell walls. In the case of the innovative cell under axial load, the end effect led to the first and second collapse shown in Figure 7, while

under lateral load, the end effect produced the characteristic shear failure in the cell mid-section, as depicted in Figure 11. For a multiple-cell arrangement, the authors expect that adjacent cells will provide mutual lateral support, tending to compensate the deformation pattern observed in the external walls of the unit cell specimens. This hypothesis will be experimentally and numerically analyzed by the authors as a continuation of the present study. Additionally, another parameter that influenced the strength and energy absorption of unit cells was the orientation of the 3D-printing layers with respect to the loading direction. Particularly, the shear failure shown in Figures 12 and 13 occurs in a plane parallel to the layer orientation. The authors believe that changing the current layer orientation would lead to an increase in strength and energy absorption in the lateral direction, while reducing them in the axial direction. However, this has not yet been experimentally verified.

As compared to the standard honeycomb configuration, the capacity to absorb more energy at the beginning of the quasi-static deformation suggests a potential improvement under dynamic loading as well; this may lead to an enhancement in aircraft passengers' safety and/or payload integrity under loads with significant lateral components. Furthermore, since the diagonal walls of the innovative geometry are enclosed within a parallelepiped shape, rectangular sandwich panels can be easily manufactured with this innovative cell, allowing reduction of the occurrence of local damages and weak points at the edges of the sandwich structure.

5. Conclusions

An innovative, non-prismatic honeycomb cell was demonstrated to be a valid alternative to standard hexagonal honeycomb in terms of energy absorption capabilities under compressive loads. Thanks to the presence of some diagonal walls (in addition to the traditional vertical walls found in conventional prismatic cells), some additional load paths are created, which allows to enhance the energy absorption. A cell with innovative geometry and a standard hexagonal cell geometry, with the same mass and height, underwent experimental and FEA compression tests, both in the axial and lateral directions. The results indicated that the innovative cell geometry offers an amount of energy absorption under lateral loads that exceeds by 15% the value measured for the standard hexagonal geometry. On the other hand, the compression tests in the axial directions indicated that the innovative cell geometry offers a level of energy absorption that is equivalent to the case of the standard hexagonal cell. This innovative honeycomb geometry can provide an enhanced level of safety in those engineering applications where loads with a significant non-normal component are expected. In addition, the external parallelepiped shape allows the tailoring of honeycomb panels that perfectly match the external boundaries of rectangular and square sandwich panels, thus reducing the risk of having weak points at the edges of the panels.

6. Patents

A US Provisional patent Application (No.: 63/299,675 Title: SCUTOIDAL SUB-CELL AND CELL ARRANGEMENTS. Application Date: 14 January 2022. Inventors: MENEGOZZO, Marco; CECCHINI BRIGI, Andres; JUST AGOSTO, Frederick A.; SERRANO ACEVEDO, David. Applicant: UNIVERSITY OF PUERTO RICO) was submitted for the innovative geometry presented in this paper.

Author Contributions: Conceptualization, M.M., A.C., F.A.J.-A. and D.S.A.; methodology, M.M., A.C., F.A.J.-A. and D.S.A.; software, A.C., M.M., F.A.J.-A., D.S.A., O.J.F.V., I.A.-F. and J.D.J.R.; validation, A.C., M.M., F.A.J.-A., I.A.-F., J.D.J.R., O.J.F.V. and D.S.A.; formal analysis, A.C., M.M., F.A.J.-A. and D.S.A.; investigation, M.M., A.C., F.A.J.-A., D.S.A., I.A.-F., J.D.J.R. and O.J.F.V.; resources, M.M., A.C., F.A.J.-A., D.S.A., O.J.F.V., I.A.-F. and J.D.J.R.; data curation, A.C., M.M., F.A.J.-A., I.A.-F., J.D.J.R., O.J.F.V. and D.S.A.; writing—original draft preparation, M.M., A.C., F.A.J.-A., D.S.A., O.J.F.V., I.A.-F. and J.D.J.R.; writing—review and editing, M.M., A.C., F.A.J.-A., D.S.A., O.J.F.V., I.A.-F. and J.D.J.R.; visualization, A.C., F.A.J.-A., J.D.J.R., O.J.F.V., I.A.-F., M.M. and D.S.A.; supervision, M.M., A.C., F.A.J.-A.

and D.S.A.; project administration, M.M., A.C., F.A.J.-A. and D.S.A.; and funding acquisition, M.M., F.A.J.-A. and D.S.A. All authors have read and agreed to the published version of the manuscript.

Funding: This research was funded by the Puerto Rico Science, Technology and Research Trust (PRSTRT), grant agreement number 2020-00135.

Institutional Review Board Statement: Not applicable.

Informed Consent Statement: Not applicable.

Data Availability Statement: Not applicable.

Acknowledgments: The undergraduate students Giancarlo Castellini-Coutin, Juan Gomez Gonzalez, Eduardo Morales Rivera, Gabriel Diaz, Paola Colon Abad, Rolando Rosales Rosete, Michael J. Ledesma Rebollo, Rolando J. Mateo Miranda, Francisco Cruz Jusino and Jesus Montañez-Saad contributed to the CAD modeling and FEM analyses of the samples. The undergraduate students Wilfredo A. Tosado Nieves, Antonio Acosta Santiago and David Negron Feliciano contributed to the execution of the experimental static compression tests. The set-up and execution of the compression tests was made possible thanks to the Civil Engineering material testing facilities of the University of Puerto Rico at Mayagüez (UPRM), and in particular thanks to the collaboration of Felipe Acosta and Iván Santiago of the UPRM Civil Engineering Department. The undergraduate student Carlos Baez Velez was the responsible of the 3D-printing activities within the research group. The additive manufacturing of the samples was made possible thanks to José E. Lugo Ortiz (Department of Mechanical Engineering, UPRM) and his research group.

Conflicts of Interest: The authors declare no conflict of interest. The funders had no role in the design of the study; in the collection, analyses or interpretation of data; in the writing of the manuscript; or in the decision to publish the results.

References

1. Tarlochan, F. Sandwich Structures for Energy Absorption Applications: A Review. *Materials* **2021**, *14*, 4731. [CrossRef] [PubMed]
2. Chen, Y.; Li, T.; Jia, Z.; Scarpa, F.; Yao, C.; Wang, L. 3D printed hierarchical honeycombs with shape integrity under large compressive deformations. *Mater. Des.* **2018**, *137*, 226–234. [CrossRef]
3. Mc Caw, J.C.S.; Cuan-Urquizo, E. Mechanical characterization of 3D printed, non-planar lattice structures under quasi-static cyclic loading. *Rapid Prototyp. J.* **2020**, *26*, 707–717. [CrossRef]
4. Li, T.; Chen, Y.; Hu, X.; Li, Y.; Wang, L. Exploiting negative Poisson's ratio to design 3D-printed composites with enhanced mechanical properties. *Mater. Des.* **2018**, *142*, 247–258. [CrossRef]
5. Townsend, S.; Adams, R.; Robinson, M.; Hanna, B.; Theobald, P. 3D printed origami honeycombs with tailored out-of-plane energy absorption behavior. *Mater. Des.* **2020**, *195*, 108930. [CrossRef]
6. Bates, S.R.G.; Farrow, I.R.; Trask, R.S. Compressive behaviour of 3D printed thermoplastic polyurethane honeycombs with graded densities. *Mater. Des.* **2019**, *162*, 130–142. [CrossRef]
7. Andrew, J.J.; Alhashmi, H.; Schiffer, A.; Kumar, S.; Deshpande, V.S. Energy absorption and self-sensing performance of 3D printed CF/PEEK cellular composites. *Mater. Des.* **2021**, *208*, 109863. [CrossRef]
8. Ma, J.; Dai, H.; Chai, S.; Chen, Y. Energy absorption of sandwich structures with a kirigami-inspired pyramid foldcore under quasi-static compression and shear. *Mater. Des.* **2021**, *206*, 109808. [CrossRef]
9. Wang, Q.; Yang, Z.; Lu, Z.; Li, X. Mechanical responses of 3D cross-chiral auxetic materials under uniaxial compression. *Mater. Des.* **2020**, *186*, 108226. [CrossRef]
10. Yang, K.; Xu, S.; Shen, J.; Zhou, S.; Xie, Y.M. Energy absorption of thin-walled tubes with pre-folded origami patterns: Numerical simulation and experimental verification. *Thin-Walled Struct.* **2016**, *103*, 33–44. [CrossRef]
11. Li, S.; Liu, Z.; Shim, V.P.W.; Guo, Y.; Sun, Z.; Li, X.; Wang, Z. In-plane compression of 3D-printed self-similar hierarchical honeycombs—Static and dynamic analysis. *Thin-Walled Struct.* **2020**, *157*, 106990. [CrossRef]
12. Qi, J.; Li, C.; Tie, Y.; Zheng, Y.; Duan, Y. Energy absorption characteristics of origami-inspired honeycomb sandwich structures under low-velocity impact loading. *Mater. Des.* **2021**, *207*, 109837. [CrossRef]
13. Guo, C.; Zhao, D.; Liu, Z.; Ding, Q.; Gao, H.; Yan, Q.; Sun, Y.; Ren, F. The 3D-Printed Honeycomb Metamaterials Tubes with Tunable Negative Poisson's Ratio for High-Performance Static and Dynamic Mechanical Properties. *Materials* **2021**, *14*, 1353. [CrossRef] [PubMed]
14. Zaharia, S.M.; Enescu, L.A.; Pop, M.A. Mechanical Performances of Lightweight Sandwich Structures Produced by Material Extrusion-Based Additive Manufacturing. *Polymers* **2020**, *12*, 1740. [CrossRef] [PubMed]
15. Basurto-Vázquez, O.; Sánchez-Rodríguez, E.P.; McShane, G.J.; Medina, D.I. Load Distribution on PET-G 3D Prints of Honeycomb Cellular Structures under Compression Load. *Polymers* **2021**, *13*, 1983. [CrossRef] [PubMed]
16. Mansour, M.T.; Tsongas, K.; Tzetzis, D. 3D Printed Hierarchical Honeycombs with Carbon Fiber and Carbon Nanotube Reinforced Acrylonitrile Butadiene Styrene. *J. Compos. Sci.* **2021**, *5*, 62. [CrossRef]

17. Sarvestani, H.Y.; Akbarzadeh, A.H.; Mirbolghasemi, A.; Hermenean, K. 3D printed meta-sandwich structures: Failure mechanism, energy absorption and multi-hit capability. *Mater. Des.* **2018**, *160*, 179–193. [CrossRef]
18. Sarvestani, H.Y.; Akbarzadeh, A.H.; Mirbolghasemi, A.; Hermenean, K. 3D printed architected polymeric sandwich panels: Energy absorption and structural performance. *Compos. Struct.* **2018**, *200*, 886–909. [CrossRef]
19. Özen, İ.; Çava, K.; Gedikli, H.; Alver, Ü.; Aslan, M. Low-energy impact response of composite sandwich panels with thermoplastic honeycomb and reentrant cores. *Thin-Walled Struct.* **2020**, *156*, 106989. [CrossRef]
20. Chen, J.; Tao, W.; Pang, S. Impact Testing of 3D Re-Entrant Honeycomb Polyamide Structure Using Split Hopkinson Pressure Bar. *Appl. Sci.* **2021**, *11*, 9882. [CrossRef]
21. Ma, N.; Deng, Q.; Li, X. Deformation Behaviors and Energy Absorption of Composite Re-Entrant Honeycomb Cylindrical Shells under Axial Load. *Materials* **2021**, *14*, 7129. [CrossRef] [PubMed]
22. Gibson, L.J.; Ashby, M.F. *Cellular Solids, Structure and Properties*, 2nd ed.; Cambridge University Press: Cambridge, UK, 1999; pp. 99–100. [CrossRef]